Energy-transfer dynamics of high-pressure rovibrationally excited molecular H_2

David J. Saiki, Sarah Cureton-Chinn,[a] Peter B. Kelly,[b),c)] and Matthew P. Augustine[b),d)]
Department of Chemistry, One Shields Avenue, University of California, Davis, California 95616

(Received 13 June 2005; accepted 12 July 2005; published online 14 September 2005)

The energy-transfer dynamics of high-pressure molecular H_2 gas initially prepared in the $|X\,^1\Sigma_g^+, v=1, J=1\rangle$ state using stimulated Raman pumping are probed with rotational Raman scattering. A computer simulation that incorporates the effects of collision-induced vibrational energy transfer is described and used to fit the experimental Raman scattering results obtained as a function of the pump/probe delay time. The $4.78\times10^{-14}\pm3.85\times10^{-16}$ $cm^3\ s^{-1}$ molecule^{-1} vibrational energy-transfer rate for decay from the $|X\,^1\Sigma_g^+, v=1, J=1\rangle$ state compares well with other lower-pressure studies. © *2005 American Institute of Physics*. [DOI: 10.1063/1.2012307]

I. INTRODUCTION

The development of theoretical models for understanding molecule-molecule interactions depends on the detailed analysis of collisional energy-transfer processes. Some of the very first work involving collisional energy redistribution provided energy-transfer cross sections but only from the ground vibrational state.[1–4] It was not until the advent of pump-probe-laser spectroscopy that the measurement of collision-induced energy-transfer rates from higher-energy vibrational and rotational states was possible.[5,6] Previous theoretical and experimental investigations of state-resolved collision-induced energy transfer have mainly revolved around determining the rate constants for a single energy-transfer event at low translational energy.[5–7] In these experimental situations, only few collisions are needed to achieve thermal equilibrium by rotational energy transfer because of the small energy gap between rotational states. To accurately study energy-level specific rotational exchange mechanisms, low sample pressures are needed as they simulate single molecule conditions. A number of investigations of the rotational energy redistribution of molecular hydrogen H_2 from the $|X\,^1\Sigma_g^+, v=1, J=1\rangle$ excited vibrational state have been probed using coherent anti-Stokes Raman spectroscopy (CARS),[6,7] resonantly enhanced multiphoton ionization,[6] and laser-induced fluorescence[5] with the main result being the measurement of the energy-transfer rates between the $|J=0\rangle$ and the $|J'=2\rangle$ rotational states and the $|J=1\rangle$ and $|J'=3\rangle$ rotational states. The effect of the exchange of vibrational energy is small on these low-pressure rotational exchange rates because the energy gap between vibrational states is large and the vibrational exchange rate is small. It is not until higher-pressure samples at rotational equilibrium are prepared that the slower detection methods such as time domain photoacoustic Raman spectroscopy (PARS) can be used to study the vibrational exchange.[8] Current theoretical models reflect these experimental constraints, specifically, vibrational energy-transfer studies at high pressure typically assume that the rotational levels have achieved thermal equilibrium.

An unanswered question with regards to low-pressure studies is whether or not state selective experimentally determined vibrational (<1 atm) and rotational (<30 torr) rate constants directly scale to high-pressure conditions like those encountered during combustion. A timely example is molecular hydrogen given the imminent conversion to a hydrogen fuel economy and that vibrational excitation has been shown to greatly effect the formation of water during H_2 combustion.[9] As these combustion systems are applied to hydrogen fuel cells,[10,11] internal combustion,[12,13] and hypersonic transport,[14,15] it will become necessary to understand the fundamentally important unexplored area of high-pressure energy dynamics.

The purpose of this work is to provide an experimental and theoretical investigation of the energy-transfer processes in >1 atm of molecular H_2 gas. A combination of stimulated Raman pumping and pure rotational Raman scattering is used to prepare and detect rovibrationally excited H_2 as a function of the delay time between the pump- and probe-laser light pulses. The experimentally determined signal intensities of all of the rotational signals detectable at room temperature are then compared to a model that includes the effects of binary molecular collisions and molecular diffusion. This combination of experiment with theory permits an experimental estimate of the rate constants for state selective vibrational exchange reactions in high-pressure H_2 gas.

II. EXPERIMENT

The experimental setup used to prepare and detect vibrationally excited hydrogen is shown in Fig. 1 and is described in detail elsewhere.[16] The essential components are two neodymium-doped yttrium aluminum garnet (Nd:YAG) lasers, a Raman shifter, and a detection system consisting of a monochromator, boxcar averager, and digitizer. The frequency-doubled 532-nm output of the first injection-seeded Nd:YAG laser (Spectra Physics GCR-270) is used to

[a)]Present address: Chemistry and Materials Science Directorate, Lawrence Livermore National Laboratory, 7000 East Avenue, Livermore, CA 94551.
[b)]Authors to whom correspondence should be addressed.
[c)]Fax: +1-530-752-8995; electronic mail: kelly@chem.ucdavis.edu
[d)]Fax: +1-530-752-8995; electronic mail: augustin@chem.ucdavis.edu

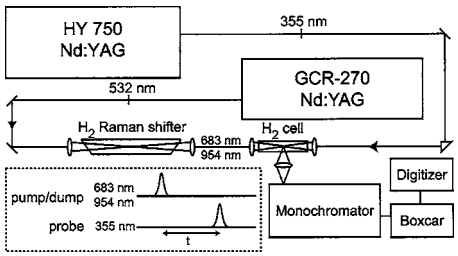

FIG. 1. Experimental setup showing the essential components in H_2 stimulated Raman pumping and rotational Raman scattering. The time delay between the 683- and 954-nm pump beams and the 355-nm probe beam is variable from 15 ns–10 μs.

pump a Raman shifter filled with 13 bar of H_2 gas. The 683- and 954-nm outputs of the Raman shifter are selected with a cut-off filter and used to pump the $|v=0\rangle \rightarrow |v=1\rangle$ Q branch transition in a separate H_2 gas sample. The second Nd:YAG laser (JK Laser HY 750) is triggered from the Q-switch gate of the first Nd:YAG laser and its 355-nm output is used to generate the rotational S branch Raman scattering from a hydrogen sample. It is possible to achieve a variable 15-ns–10-μs time delay between the pump and probe pulses by adjusting the Q-switch timing of the second laser. Examples of the performance of this experimental setup applied to the rotational S branch of H_2 gas following Q branch pumping are shown in Fig. 2.

The intensity of each scattering signal in the spectra shown in Fig. 2 was determined by fitting each peak to a Gaussian function as the noise level in Fig. 2 concealed the low intensity shoulders of the anticipated Lorentzian profile. The area of each of these Gaussians was used to compare the experimental results to the model discussed in Sec. III. All error estimates were obtained by comparing the best-fit parameters determined by a minimization of the sum of mean-square differences between the data and the fit function ϵ to parameters determined by fitting the spectra for the second time to identify parameter values when a 1.05ϵ value is achieved.

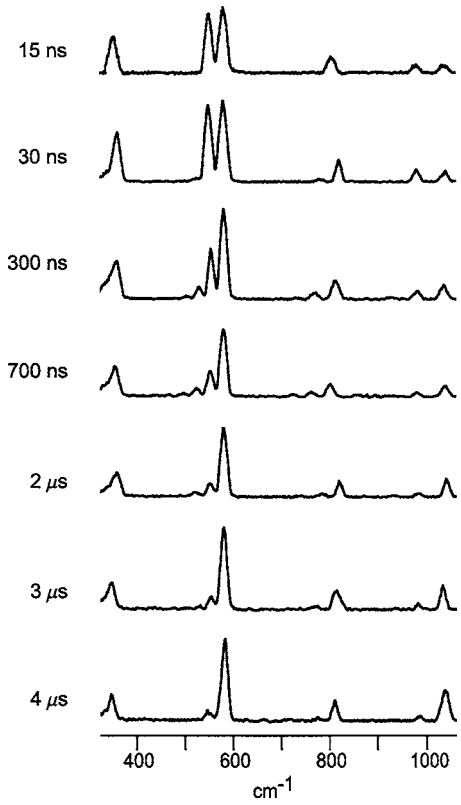

FIG. 2. Rotational Raman spectra of the S branch of H_2 plotted as a function of pump/probe delay time following the excitation to the $|v=1,J=1\rangle$ state. The signals centered at 354.37, 587.09, 814.45, and 1034.69 cm^{-1} represent Raman scattering from the $|v=0,J=0,1,2,\text{and } 3\rangle$ states, respectively, while the additional peaks represent scattering from higher vibrational states.

III. ENERGY-TRANSFER MODEL

The development of a model to simulate vibrational energy transfer in molecular H_2 gas is motivated by the experimental results shown in Fig. 2. Here the S branch rotational Raman spectrum of molecular H_2 is scanned at the time t following stimulated Raman pumping of the $|v=1,J=1\rangle$ state in the $^1\Sigma_g^+$ ground state of H_2 gas at the time $t=0$. It is these $I(t)_{|v,J\rangle}$ S branch scattering signals that allows energy transfer from the originally pumped $|v=1,J=1\rangle$ state to other $|v',J'\rangle$ states to be tracked. The intensity of each S branch rotational Raman transition $I(t)_{|v,J\rangle}$ can be related to the average number density of molecules in a given $|v,J\rangle$ state $\bar{N}(t)_{|v,J\rangle}$ by the appropriate product of rotational- and nuclear-spin degeneracy factors and the polarizability anisotropy[17] $\gamma_{vv,JJ+2}$ as $I(t)_{|v,J\rangle}=(2J+1)(2I+1)(\gamma_{vv,JJ+2})^2\bar{N}(t)_{|v,J\rangle}$. In this way the scattering intensity is scaled with respect to the product $(\gamma_{vv,JJ+2})^2\bar{N}(t)_{|v,J\rangle}$ by the numerical degeneracy factors of 1, 9, 5, and 21 for the $S_{vv}(0)$, $S_{vv}(1)$, $S_{vv}(2)$, and $S_{vv}(3)$ lines, respectively.[16] The use of the average state number density $\bar{N}(t)_{|v,J\rangle}$ anticipates both the dynamics of the energy-transfer data shown in Fig. 2 and the spatial aspects of the experiment that involve focusing both the pumping and detection laser beams into a large volume of H_2 gas.

Consider first the drastically different time scales for rotational and vibrational energy transfer. Scaling Farrow and Chandler's[6] low-pressure single molecule rate for the $|J=1\rangle \rightarrow |J=3\rangle$ rotational energy-transfer rate up to 2 atm yields a rate of 8.0×10^7 s^{-1} suggesting a time constant of 13 ns, a time comparable to the delay between the pump- and probe-laser pulses for the top spectrum shown in Fig. 2. The presence of the $|v=1,J=3\rangle$ scattering signal at $\approx$980 cm^{-1} for $t=15$ ns in Fig. 2 suggests that a quasiequilibrium amongst the rotational states is created due to rapid rotational energy transfer while the slower process of vibrational energy transfer proceeds towards true thermal equilibrium. The idea of rotational quasiequilibrium was originally postulated in the PARS-based vibrational energy-transfer work of Kruetz *et al.*,[8] but that method did not have the rotational state resolution to support the idea. A closer inspection of the spectra in Fig. 2 indicates that the short-time quasiequilibrium amongst rotational states is not complete as the scattering signal for the $|v=1,J=2\rangle$ state at $\approx$760 cm^{-1} does not appear until $t=30$ ns and the appearance and disappearance rates of the even and odd J or equivalently the para and ortho states are different. This observation suggests that two separate quasiequilibrium conditions exist—one for the nuclear spin $I=0$

para states and one for the $I=1$ ortho states. The spectra shown in Fig. 2 are consistent with the idea that energy is exchanged between these spin manifolds by vibrational energy transfer.[18] The consequence of this observation implies that the treatment of energy transfer in high-pressure H_2 gas is greatly simplified because only the two para and ortho nuclear-spin manifolds must be considered instead of the usual $J_{\max}$ levels anticipated on the basis of the individual state number densities $\bar{N}(t)_{|v,J\rangle}$ and the entire rotational Raman spectrum. Straightforward application of this simplification allows the average number density $\bar{N}(t)_{|v,J\rangle}$ to be written in terms of the total H_2 number density N_{H_2} and the vibrational state dependent average para and ortho population $\bar{P}(t)_{|v,I\rangle}$ as

$$\bar{N}(t)_{|v,J\rangle} = N_{H_2} B_{|v,J,I\rangle} \bar{P}(t)_{|v,I\rangle}, \tag{1}$$

where the abbreviated Boltzmann factor $B_{|v,J,I\rangle}$ for the $I=0$ para or the $I=1$ ortho quasiequilibrium in terms of the energy of the $|v,J\rangle$ state $E_{|v,J\rangle}$, the Boltzmann constant k, and the temperature T is given by

$$B_{|v,J,I\rangle} = \frac{(2J+1)(2I+1)e^{E_{|v,J\rangle}/kT}}{Z_{|v,I\rangle}}. \tag{2}$$

The partial partition function

$$Z_{|v,I\rangle} = \sum_{J=0}^{J_{\max}} (4J+2I+1)(2I+1)e^{E_{|v,2J+1\rangle}/kT} \tag{3}$$

only considers the para or ortho states within a given vibrational level. When written in this way it should be clear that the $\bar{P}(t=\infty)_{|v,I\rangle}$ thermal equilibrium population is $Z_{|v,I\rangle}$ and can be determined from a sum of the standard degeneracy-weighted Boltzmann factors, here the numerator in Eq. (2), for all of the para states within a given vibrational state $|v\rangle$ when $I=0$ while the sum extends over all of the ortho states when $I=1$.

Next consider the meaning of the average population $\bar{P}(t)_{|v,I\rangle}$. The stimulated Raman pumping laser profile in a gaseous sample defines the state population at the time $t=0$ as $P(\mathbf{r},t=0)_{|v,I\rangle}$ and the 355-nm detection laser profile $g(\mathbf{r})$ determines the fraction of $P(\mathbf{r},t)_{|v,I\rangle}$ that is measured by the experiment. When defined in this way the average para and ortho population in the $|v\rangle$ state at any time t becomes $\bar{P}(t)_{|v,I\rangle} = \int P(\mathbf{r},t)_{|v,I\rangle} g(\mathbf{r}) d\mathbf{r}$. The treatment of the dynamics of the S branch rotational Raman spectrum of H_2 following stimulated Raman pumping is therefore equivalent to the description of the time behavior of each para and ortho state population $P(\mathbf{r},t)_{|v,I\rangle}$, here considered as individual elements of a $2(v_{\max}+1)\times 1$-dimensional column vector $\mathbf{P}(\mathbf{r},t)$ representing the full population at the position $\mathbf{r}$ and the time t. The change in this population vector as a function of time can be described by a master equation involving only two principal terms as

$$\frac{d}{dt}\mathbf{P}(\mathbf{r},t) = -\Gamma{:}\mathbf{P}(\mathbf{r},t)\mathbf{P}(\mathbf{r},t) + \mathbf{D}\nabla^2\mathbf{P}(\mathbf{r},t), \tag{4}$$

where Γ is a third-rank cartesian tensor or exchange matrix and D is the self-diffusion constant for molecular H_2 gas. The first term in Eq. (4) proportional to Γ reflects the highest probability energy-transfer event due to binary collisions. Although collisions involving three or more H_2 molecules are likely to occur in the high-pressure gas considered here, the energy-transfer dynamics will still be dominated by two particle collisions. Incorporation of diffusion into the second term in Eq. (4) accounts for molecular motion on the time scale of the experiment in addition to including the possibility of nonuniform sample excitation and detection as mentioned above.

IV. THE EXCHANGE MATRIX

Before proceeding with the actual construction of the exchange matrix Γ, it is important to pause and consider the physical meaning of its elements. As a starting point the first-order perturbation energies for the diatomic vibrational and rotational Hamiltonian and thus the zeroth-order wave functions $|v,J\rangle$ are taken to constitute the eigenenergies and eigenbasis, respectively. Furthermore, as mentioned above, the time scale of the experiment precludes the measurement of rotational energy transfer therefore the number of rotational levels that need to be considered collapses to the two $I=0$ and $I=1$ nuclear-spin states, thus defining the effective state $|v,I\rangle$. Regardless of the number of molecules involved in a collision, the population of a target $|v,I\rangle$ effective state $P(\mathbf{r},t)_{|v,I\rangle}$ will either be produced or consumed during an energy-transfer event. In the special case considered here involving just two molecules, the target $|v,I\rangle$ effective state population $P(\mathbf{r},t)_{|v,I\rangle}$ is produced by the collision of one molecule in the $|v_r,I_r\rangle$ effective state with another molecule in the $|v_r',I_r'\rangle$ effective state. A collision between a molecule in the $|v,I\rangle$ effective state with another molecule in the $|v_r,I_r\rangle$ effective state can consume $P(\mathbf{r},t)_{|v,I\rangle}$ population by producing molecules in the $|v_p,I_p\rangle$ and $|v_p',I_p'\rangle$ effective states. It should be clear that the r and p subscripts on the vibrational v and nuclear-spin I quantum numbers refer to reactant and product molecules in an energy-transfer reaction. Both the production and consumption of $|v,I\rangle$ effective state population $P(\mathbf{r},t)_{|v,I\rangle}$ due to these exchange processes can be summarized with a transfer matrix K. The columns of this transfer matrix K are labeled as the $|v_r,I_r;v_r',I_r'\rangle$ reactants while the rows are designated by the $\langle v_p,I_p;v_p',I_p'|$ products. The assignment of the matrix elements of K is reserved for Sec. V. Since the matrix K relates reactants to products, the exchange contribution to the $|v,I\rangle$ effective state population can be written as

$$\frac{d}{dt}P(\mathbf{r},t)_{|v,I\rangle} = \sum_{\substack{v_r,I_r \\ v_r',I_r' \\ v_p,I_p}} (\langle v,I;v_p,I_p|K|v_r,I_r;v_r',I_r'\rangle + \langle v_p,I_p;v,I|K|v_r,I_r;v_r',I_r'\rangle)P(\mathbf{r},t)_{|v_r,I_r\rangle}P(\mathbf{r},t)_{|v_r',I_r'\rangle}$$
$$- \sum_{\substack{v_r,I_r \\ v_p,I_p \\ v_p',I_p'}} (\langle v_p,I_p;v_p',I_p'|K|v,I;v_r,I_r\rangle + \langle v_p,I_p;v_p',I_p'|K|v_rI_r;v,I\rangle)P(\mathbf{r},t)_{|v,I\rangle}P(\mathbf{r},t)_{|v_r,I_r\rangle}. \quad (5)$$

In principle the matrix K has infinite dimension, however for computational purposes the dimensionality is reduced to a size set by the two ortho and para nuclear-spin states and the maximum number of vibrational $v_{\max}+1$ levels considered in a real computation of the dynamics of the exchanging H_2 system. For example, if the number of vibrational levels is set to four then the matrix K contains $(4\times2)^4=4096$ elements of which most are zero. Since the exchange matrix approach is computationally inefficient, the alternative tensor contraction shown in Eq. (4) involving only $(4\times2)^3=512$ matrix elements for the $v_{\max}=3$ four vibrational level system can be used to streamline the calculation of the $|v,I\rangle$ effective state population due to exchange as

$$\frac{d}{dt}P(\mathbf{r},t)_{|v,I\rangle} = \sum_{\substack{V_r,I_r \\ v_r',I_r'}} \Gamma(v,I;v_r,I_r;v_r',I_r')P(\mathbf{r},t)_{|v_r,I_r\rangle}P(\mathbf{r},t)_{|v_r',I_r'\rangle}. \quad (6)$$

A comparison of Eq. (5) to Eq. (6) dictates that the matrix elements of the tensor Γ can be related to the more physical transfer matrix K as

$$\Gamma(v,I;v_r,I_r;v_r',I_r') = \sum_{\substack{v_p,I_p \\ v_p',I_p'}} \langle v_p,I_p;v_p',I_p'|K|v_r,I_r;v_r',I_r'\rangle \times(\delta_{v_p,v}\delta_{I_p,I} + \delta_{v_p',v}\delta_{I_p',I} - \delta_{v_r,v}\delta_{I_r,I} - \delta_{v_r',v}\delta_{I_r',I}). \quad (7)$$

Provided that the elements of the matrix K are known, the projection shown in Eq. (7) can be used to determine the matrix elements of Γ and thus used to model the energy-transfer dynamics in H_2 with Eq. (4). The matrix form for the total transfer matrix K can be separated into a vibrational and nuclear spin or projected rotational contribution because the $|v,J\rangle$ eigenstates are really constructed from a product of the vibrational wave function $|v\rangle$ with the rotational wave function $|J\rangle$. The reduced dimensionality of these separate problems greatly simplifies the construction of the full transfer matrix K from a basis set expansion of just the vibrational exchange matrix K_{vib} as described in Sec. V.

V. VIBRATIONAL EXCHANGE

The matrix elements of the vibrational transfer matrix K_{vib} correspond to the probability of a collision-mediated reaction occurring between molecules in the $|v_r\rangle$ and $|v_r'\rangle$ states to form molecules in the $|v_p\rangle$ or $|v_p'\rangle$ states. Given that a molecule can be in any $|v_r\rangle$ or $|v_r'\rangle$ state the dominant $\Delta v=\pm1$ selection rule dictates that during a two-body collision, one molecule must give up one quantum of energy while the other molecule must absorb that quantum of energy. In terms of the collision reaction, the selection rule means that $|v_r\rangle\rightarrow|v_r\pm1\rangle$ while $|v_r'\rangle\rightarrow|v_r'\mp1\rangle$. In practice the columns of the vibrational transfer matrix K_{vib} are labeled by the vibrational quantum number of the reacting molecules $|v_r,v_r'\rangle$, while the rows indicate the vibrational quantum numbers of the products $\langle v_p,v_p'|$. Therefore, in the absence of rotational energy transfer the $\langle v_p,v_p'|K_{\text{vib}}|v_r,v_r'\rangle$ matrix element describes both the probability of the reaction and the change in the $P(\mathbf{r},t)_{|v\rangle}$ state population due to a mixing with both the $P(\mathbf{r},t)_{|v_r\rangle}$ and $P(\mathbf{r},t)_{|v_r'\rangle}$ state populations. All of the matrix elements of K_{vib} are scaled to a common probability or exchange rate W_{vib} that is obtained by comparison of theory to experimental data. This rate is proportional to the cross section for vibrational exchange and specifically corresponds to the process

$$v_r=0+v_r'=1 \overset{W_{\text{vib}}}{\rightarrow} v_p=1+v_p'=0, \quad (8)$$

where the $|v_p=1\rangle$ state is generated from the $|v_r=0\rangle$ state while the $|v_p'=0\rangle$ state is produced from the $|v_r'=1\rangle$ state during a collision. The collision reaction in Eq. (8) contributes $+W_{\text{vib}}$ to the $\langle0,1|K_{\text{vib}}|1,0\rangle$ and $\langle1,0|K_{\text{vib}}|0,1\rangle$ matrix elements. A general relation for the matrix elements of K_{vib} can be developed by considering two additional collision-mediated vibrational exchange reactions

$$v_r=1+v_r'=2 \overset{3W_{\text{vib}}}{\rightarrow} v_p=0+v_p'=3 \quad (9)$$

and

$$v_r=0+v_r'=2 \overset{2W_{\text{vib}}}{\rightarrow} v_p=1+v_p'=1. \quad (10)$$

Here the nonzero matrix elements of K_{vib} are $\langle0,3|K_{\text{vib}}|1,2\rangle=\langle3,0|K_{\text{vib}}|2,1\rangle=+3W_{\text{vib}}$ for Eq. (9) and $\langle1,1|K_{\text{vib}}|2,0\rangle=\langle1,1|K_{\text{vib}}|0,2\rangle=+2W_{\text{vib}}$ for Eq. (10). In general the scaling factors multiplying W_{vib} that constitute the matrix elements of K_{vib} relate to the square of the matrix elements of the ladder operators $a_ia_j^\dagger$ and $a_m^\dagger a_n$, where $a_k|v_k\rangle=v_k^{1/2}|v_k-1\rangle$ and $a_k^\dagger|v_k\rangle=(v_k+1)^{1/2}|v_k+1\rangle$.[19] Since the matrix elements of K_{vib} are proportional to the square of the ladder operator elements, the alternative forms $\tilde{a}|v\rangle=v|v-1\rangle$ and $\tilde{a}^\dagger|v\rangle=(v+1)|v+1\rangle$ are used here. Each op-

erator $\tilde{a}_k$ and $\tilde{a}_k^\dagger$ spans just one set of vibrational wave functions $|v_k\rangle$, therefore the operator K_{vib} that leads to the appropriate vibrational exchange matrix can be written as

$$K_{\text{vib}} = (\tilde{a}_r \tilde{a}_{r'}^\dagger + \tilde{a}_r^\dagger \tilde{a}_{r'}) W_{\text{vib}}, \tag{11}$$

where the operators $\tilde{a}_r$, $\tilde{a}_{r'}$, $\tilde{a}_{r'}^\dagger$, and $\tilde{a}_{r'}^\dagger$ can be expressed in the $|v_r, v_r'\rangle$ basis from a Kronecker product expansion of the matrices for $\tilde{a}$, $\tilde{a}^\dagger$, and the unit matrix E that span the $|v\rangle$ states as

$$\begin{aligned} &\tilde{a}_r = \tilde{a} \otimes E, \quad \tilde{a}_{r'} = E \otimes \tilde{a}, \\ &\tilde{a}_r^\dagger = \tilde{a}^\dagger \otimes E, \quad \tilde{a}_{r'}^\dagger = E \otimes \tilde{a}^\dagger. \end{aligned} \tag{12}$$

In the absence of rotational level structure Eqs. (12) can be used with Eq. (11) to determine the matrix form for K_{vib} and ultimately describe vibrational energy transfer via the matrix Γ in Eq. (7), where the $I=0$ and $I=1$ para and ortho states are not included.

In the presence of nuclear spin, the problem is slightly more complex. Again a basis set expansion can be used to expand the $|v_r, v_r'\rangle$ basis set that spans K_{vib} into the $|v_r, I_r; v_r', I_r'\rangle$ basis. Here the 4×4 unit matrix E_{spin} accounting for the four possible combinations of ortho and para collisions combined with an outer product expansion can be used to expand K_{vib} into the full spin-vibrational basis $|v_r, I_r; v_r', I_r'\rangle$ as $K_{\text{vib}} \otimes E_{\text{spin}}$. This basis set expansion will account for $\Delta v = \pm 1$ energy-transfer processes in the presence of spin when ortho/para conversion is forbidden during a collision. For the specific case of the two-body collisions shown in Eqs. (9) and (10), this expansion generates the appropriate vibrational contribution for the processes

$$v_r = 1, I_r + v_r' = 2, I_r' \overset{3W_{\text{vib}}}{\rightarrow} v_p = 0, I_r + v_p' = 3, I_r' \tag{13}$$

and

$$v_r = 0, I_r + v_r' = 2, I_r' \overset{2W_{\text{vib}}}{\rightarrow} v_p = 1, I_r + v_p = 1, I_r'. \tag{14}$$

Unfortunately this crude model for vibrational exchange in the presence of nuclear spin is not valid because of the symmetry imparted on the molecular wave functions by the nuclear spin. A collision between two H_2 molecules can involve molecules of the same or opposite nuclear-spin symmetry. Therefore, there are four different possibilities for the nuclear-spin symmetry involved in a binary collision, here labeled as o-o, p-p, o-p, and p-o for the ortho/ortho, para/para, ortho/para, and para/ortho combinations, respectively. These four possibilities can be accounted for in the basis set expansion of K_{vib} into the full dimensionality of the problem by defining the nonzero o-o, p-p, o-p, and p-o subcomponents of the E_{spin} "unit matrix" that selects for the states involving ortho/ortho, para/para, ortho/para, and para/ortho collisions as

$$\begin{aligned} &\langle 0,0|E_{\text{spin}}^{\text{p-p}}|0,0\rangle = 1, \quad \langle 0,1|E_{\text{spin}}^{\text{o-o}}|0,1\rangle = 1 \\ &\langle 1,1|E_{\text{spin}}^{\text{o-o}}|1,1\rangle = 1, \quad \langle 1,0|E_{\text{spin}}^{\text{o-p}}|1,0\rangle = 1. \end{aligned} \tag{15}$$

By introducing the scaling factors $a_{\text{o-o}}$, $a_{\text{p-p}}$, $a_{\text{o-p}}$, and $a_{\text{p-o}}$ that vary between 0 and 1, the expansion matrix E_{spin} can be rewritten as

$$E_{\text{spin}} = a_{\text{o-o}} E_{\text{spin}}^{\text{o-o}} + a_{\text{p-p}} E_{\text{spin}}^{\text{p-p}} + a_{\text{o-p}} E_{\text{spin}}^{\text{o-p}} + a_{\text{p-o}} E_{\text{spin}}^{\text{p-o}}. \tag{16}$$

Clearly in the limit that all of the "a" coefficients are equal to 1, the matrix for E_{spin} reduces to a true unit matrix or the case involving no nuclear-spin symmetry considerations. In the most general case however, E_{spin} will have nonzero values for the a coefficients that can be used to determine the vibrational contribution to K as

$$\begin{aligned} K = {} & a_{\text{o-o}} K_{\text{vib}} \otimes E_{\text{spin}}^{\text{o-o}} + a_{\text{p-p}} K_{\text{vib}} \otimes E_{\text{spin}}^{\text{p-p}} + a_{\text{o-p}} K_{\text{vib}} \otimes E_{\text{spin}}^{\text{o-p}} \\ & + a_{\text{p-o}} K_{\text{vib}} \otimes E_{\text{spin}}^{\text{p-o}}. \end{aligned} \tag{17}$$

This matrix is a function of the separate parameters $a_{\text{o-o}} W_{\text{vib}}$, $a_{\text{p-p}} W_{\text{vib}}$, $a_{\text{o-p}} W_{\text{vib}}$, and $a_{\text{p-o}} W_{\text{vib}}$, the vibrational exchange rates for the same and different symmetry collisions, processes that ultimately relate the different $P(\mathbf{r}, t)_{|v,I\rangle}$ elements in Eq. (4) via Eq. (7).

VI. COMPARISON TO EXPERIMENT

The first step in a comparison of theory to experiment is the determination of spectral intensities from the rotational Raman spectra in Fig. 2. The rotational Raman scattering signals in each spectrum in Fig. 2 were fit to a collection of Gaussian peaks whose areas were calculated to obtain relative integrated signal intensities for each observed transition. The Raman cross sections[16,17] were divided out of these intensities to obtain the relative populations of each energy level. In this way the ratio $\bar{N}(t)_{|v,J\rangle}/N_{H_2}$ can be compared to the calculation of $\bar{P}(t)_{|v,I\rangle}$ via Eq. (1).

Before discussing this normalized data few comments regarding the raw data in Fig. 2 are warranted. For the 15-ns delay, it is evident that some of the original $|v=1, J=1\rangle$ population has been transferred into the $|v=1, J=3\rangle$ state. This population growth can be attributed to the rapid rotational energy transfer between the $|v=1, J=1\rangle$ and $|v=0, J=3\rangle$ states, because following stimulated Raman pumping at $t=0$, these two states have the largest population of any state that can participate in $\Delta J = \pm 2$ rotational energy transfer. Thus, the $|v=1, J=3\rangle$ scattering signal decreases at $t=30$ ns following stimulated Raman pumping and vibrational population transfer between neighboring rotational states dominates, resulting in a decrease of the $|v=1, J=3\rangle$ state population. At slightly longer times, population is observed in the $|v=1, J=2\rangle$ state as well as in higher vibrational levels within the $|J=1\rangle$ state. In fact, this population pooling results in resolvable Raman scattering signals all the way up to the $|v=4, J=1\rangle$ state. The transfer of energy between the $|J=1\rangle$ and $|J=2\rangle$ rotational states appears to be an ortho-para hydrogen conversion, however, one should realize that this is simply due to vibrational energy transfer between the excited $|v=1, J=1\rangle$ state and the ground $|v=0, J=2\rangle$ state and there is no rotational energy being exchanged. It is also important to note that the energy transferred into the $|J=0\rangle$ rotational state cannot be tracked with vibrational state resolution as the separation between the Raman scattering signals from different vibrational states is below the monochromator resolution. Finally, at long times t following stimulated Raman

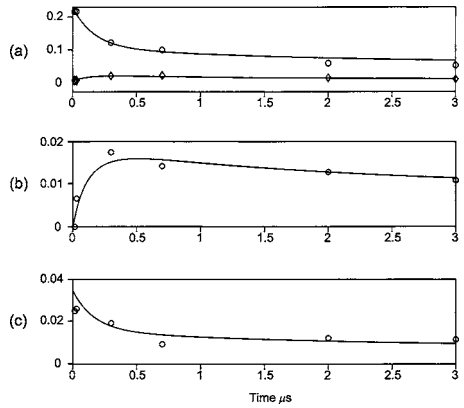

FIG. 3. Time traces of the populations of (a) the $|v=1\rangle$ (circles) and $|v=2\rangle$ (diamonds) states within the $|J=1\rangle$ manifold, (b) the $|v=1,J=2\rangle$ state, and (c) the $|v=1,J=3\rangle$ state. The solid lines represent the simulated time dependence of these states as a result of vibrational energy transfer.

pumping, Boltzmann relaxation dominates the exchange processes and the populations of all the rovibrational states approach their equilibrium values.

The normalized data shown in Fig. 3 as points represent the degeneracy-weighted populations from the $|v>0,J=1,2,$ and $3\rangle$ rotational states obtained from the Raman spectrum in Fig. 2 while the solid lines represent the results of a numerical simulation using the model outlined above for the six lowest H_2 vibrational states. The experimental error in the determination of the normalized data is less than the size of the point in Fig. 3. The best agreement between the simulation and the data uses $D=8.82\times10^{-5}\pm3.33\times10^{-7}$ m^2 s^{-1}, $W_{\mathrm{vib}}=2.69\times10^{6}\pm8.03\times10^{4}$ s^{-1}, $a_{\mathrm{o\text{-}o}}=1.11\times10^{-1}\pm3.88\times10^{-3}$, $a_{\mathrm{p\text{-}p}}=1.02\times10^{-3}\pm2.57\times10^{-5}$, $a_{\mathrm{o\text{-}p}}=8.69\times10^{-1}\pm4.40\times10^{-2}$, and $a_{\mathrm{p\text{-}o}}=1.88\times10^{-2}\pm9.58\times10^{-4}$ values. The time steps and spatial points used in the calculation were appropriate for a total pump/probe delay time of 3 μs, a pump beam waist of 29 μm, and detection beam waist of 2 μm. It is clear that the simulation reliably reproduces the features of the experimental data, namely, fast vibrational transfer and slower decay due to diffusional loss of excited state number density from the detection beam volume. At long times t following stimulated Raman pumping, the vibrational energy exchange processes manifest themselves as an increase of the $|v=1,J=2\rangle$ state population $\bar{N}(t)_{|v=1,J=2\rangle}/N_{\mathrm{H_2}}$ clearly shown in Fig. 3(b) and the population of the higher vibrationally excited states within the $|J=1\rangle$ manifold of states $\bar{N}(t)_{|v,J=1\rangle}/N_{\mathrm{H_2}}$ shown in Fig. 2. The reduced data shown in Fig. 3 is consistent with the collisional nuclear-spin symmetry parameters extracted from the simulation and shown in Table I. The largest of these factors corresponds to collisions between either all ortho molecules $a_{\mathrm{o\text{-}o}}$ or between ortho and para molecules $a_{\mathrm{o\text{-}p}}$, consistent with the $|v=1,J=3\rangle$ scattering signal at the time $t=15$ ns and the $|v=1,J=2\rangle$ scattering signal at the time $t=30$ ns in Fig. 2. The smaller $a_{\mathrm{p\text{-}p}}$ and $a_{\mathrm{p\text{-}o}}$ coefficients for collisions between para molecules and para and ortho molecules allows for the longer time buildup of population in higher vibrational levels for $J=1$, 2, and 3 in Fig. 2. The fact

TABLE I. General rates and symmetry scaling parameters obtained from the energy-transfer model and scaled to represent a single molecule. These rates may be scaled appropriately to obtain the rate for any given vibrational energy-transfer process.

Parameter		Value
Vibrational exchange	W_{vib}	$5.55\times10^{-14}\pm1.64\times10^{-7}$ cm^3 s^{-1} molecule^{-1}
Symmetry parameter	$a_{\mathrm{o\text{-}o}}$	$1.11\times10^{-1}\pm3.88\times10^{-3}$
	$a_{\mathrm{p\text{-}p}}$	$1.02\times10^{-3}\pm2.57\times10^{-5}$
	$a_{\mathrm{o\text{-}p}}$	$8.69\times10^{-1}\pm4.40\times10^{-2}$
	$a_{\mathrm{p\text{-}o}}$	$1.88\times10^{-2}\pm9.58\times10^{-4}$

that the simulation provides a larger value for $a_{\mathrm{o\text{-}p}}$ in comparison to $a_{\mathrm{p\text{-}o}}$ anticipates the equilibrium 3:1 concentration of ortho:para molecules.

The vibrational rate used to model the data in Fig. 3 can be scaled to represent the exchange rate for a single molecule as $W_{\mathrm{vib}}=5.55\times10^{-14}\pm1.64\times10^{-15}$ cm^3 s^{-1} molecule^{-1} by dividing out the H_2 number density at 2 atm pressure. These single molecule rates in addition to the symmetry scaling factors used for vibrational exchange are summarized in Table I. The W_{vib} single molecule rate can be used in combination with the appropriate state dependent scaling factors to assign rates for single reactions from the $|v=1,J=1\rangle$ state to the $|v,J\rangle$ state $W_{11,vJ}$. Specifically, $W_{11,21}=2a_{\mathrm{o\text{-}o}}W_{\mathrm{vib}}=1.22\times10^{-14}\pm7.91\times10^{-16}$ cm^3 s^{-1} molecule^{-1} and $W_{11,12}=a_{\mathrm{o\text{-}p}}W_{\mathrm{vib}}=4.78\times10^{-14}\pm3.85\times10^{-15}$ cm^3 s^{-1} molecule^{-1} where the scaling factors are described above.

It is important to comment on the meaning of the diffusion term in Eq. (4) and how the term leads to the long-time damping of the calculated signal in Fig. 3 but not to the appropriate Boltzmann equilibrium $|v,J\rangle$ state population. To begin, the 3-μs duration of the experiment combined with the $D=8.82\times10^{-5}\pm3.33\times10^{-7}$ m^2 s^{-1} self-diffusion coefficient for H_2 gas used to obtain the best fit of simulation to experiment shown in Fig. 3 implies that the root-mean-square displacement of a given molecule is approximately $(Dt)^{1/2}=1.63\times10^{+1}\pm3.06\times10^{-2}$ μm, a distance comparable to both the 2-μm, 355-nm detection beam waist and the 29-μm stimulated Raman pumping beam waist. As a comparison, the slightly smaller literature value for the room-temperature H_2 gas diffusion coefficient $D=6.49\times10^{-5}$ m^2 s^{-1} yields a marginally shorter root-mean-square displacement of $1.40\times10^{+1}$ μm.[20] The decay noticed in the solid lines in Fig. 3 is primarily a reflection of the ≈50% loss of $|v=1,J=1\rangle$ state population due to molecular migration out of both the prepared and monitored sample volume. But, the decay of the vibrational excitation in the probed volume is not that simple as shown in Eq. (4). The diffusion of thermal equilibrium molecules into the probed volume also contributes to the decay as the exchange contribution to the dynamics of the $P_{|v,J\rangle}$ population mixes the excited-state population remaining in the probed volume at the time t with the new thermal equilibrium population that migrated into the volume. Given that the ratio of the probed sample volume to the ≈50-cm^3 sample volume is $\approx10^8$ positional equilibration of the excited-state number density has not occurred in the 3-μs duration of the experiment as shown in Fig. 3(c), where the

TABLE II. Comparison of vibrational energy-transfer rates from the $|v=1,J=1\rangle$ state of H_2 obtained here to literature values. The reactions are written in terms of vibrational and rotational $|v,J\rangle$ state.

Reaction $\|v,J\rangle$	Rate ($cm^3\ s^{-1}$ molecule^{-1})	Method	Source
$1,1+0,2\rightarrow 0,1+1,2$	$7.07\times10^{-14}\pm2.98\times10^{-14}$	CARS	Ref. 6
$W_{11,12}$	$4.78\times10^{-14}\pm3.85\times10^{-15}$	transfer model	This work
$1,1+1,1\rightarrow 2,1+0,1$	$2.5\times10^{-14}\pm1.50\times10^{-14}$	PARS	Ref. 8
$W_{11,21}$	$1.22\times10^{-14}\pm7.91\times10^{-16}$	transfer model	This work

$|v=1,J=3\rangle$ population does not approach equilibrium. In this case it is safe to ignore the approach of $P_{|v,J\rangle}$ sample population to the true Boltzmann equilibrium values anticipated at room temperature at the time $t=\infty$ after application of the stimulated Raman pumping pulse. A true nonphenomenological account of the approach of the sample energetics to Boltzmann equilibrium requires a higher level of theory as well as experiments on larger volumes and extension of the measurements to millisecond or second time scales where diffusion has established a state of positional equilibrium.

Finally, consider the comparison of the single state energy-transfer rates used in the numerical simulation $W_{11,vJ}$ to the low-pressure literature values shown in Table II. It is comforting to realize that the $W_{11,vJ}$ values reported in Table II at high pressure are within the range of the low-pressure values. Any deviation between pressure-dependent values could be due to the fact that the rates measured here at 2 atm pressure are scaled to represent a single molecule collision or that the assignment of specific energy-transfer events as is typical for low-pressure studies is not appropriate at 2 atm. In reality the high-pressure rates correspond to more than just one energy-transfer reaction—possibilities included in the simulated rates. The agreement between low- and high-pressure values in Table II is interesting given that the $W_{11,vJ}$ values quoted in this study were obtained from a comparison of experiment to a simulation limited to just binary two-body collisions. At high pressure, ternary and higher-order multiple collision events are occurring and contributing to the overall observable vibrational transfer rate. These higher-order multiple collision events could be modeled in the current theoretical framework by including higher rank tensor contractions. However, before undertaking such an arduous task, an experimental determination of the presence of these collisions at lower pressures must be performed to determine at what pressure the rotational quasiequilibrium is valid. Further improvements to the simulation could also be made by including rovibrational $|v,J\rangle$-state mixing, an effect that essentially introduces $|\Delta v|>1$ transitions. Of course spectroscopically available parameters can be used to estimate the degree of rovibrational coupling in H_2 gas, and again the simulation could be modifed here by expanding the dimensionality of the vibrational exchange matrix as $K_{\mathrm{vib}} \propto (\tilde{a}_r\tilde{a}_{r'}^{\dagger})^n+(\tilde{a}_r^{\dagger}\tilde{a}_{r'})^n$, where n is the number of vibrational quanta involved in the energy exchange. Although the simulation used in this study is admittedly primitive, the recovery of low-pressure energy-transfer rates gives some confidence in the ability to predict the dynamics of vibrational energy transfer at high pressure. It is the study and understanding of molecular systems in realistic environments that will provide insight into energy-transfer kinetics in fundamentally important systems relying on energy exchange like H_2+O_2 combustion where it is known that H_2 vibrational excitation can increase the combustion rate by two orders of magnitude.[21]

VII. CONCLUSIONS

The vibrational energy exchange from the $|X\,^1\Sigma_g^+, v=1,J=1\rangle$ state of molecular H_2 at 2 atm pressure has been measured. Additionally, a theoretical model that incorporates all possible vibrational transfer mechanisms within the lowest six vibrational states of molecular H_2 has been developed and applied to experimental data. Using this model, one can estimate the transfer rate into or out of any rovibrational state. Although this technique shows great promise for bulk studies of high-pressure gas systems, a more detailed experimental study of the energy-transfer dynamics is warranted. One experiment involves replacing the monochromator-based detection system with a charge-coupled device (CCD) array. In this way the entire rotational Raman spectrum could be captured at once thus eliminating the primary source of error in the current study. Additionally the use of a liquid-nitrogen-cooled Raman shifter to pump the $|X\,^1\Sigma_g^+,v=1, J=0\rangle$ state in H_2 will yield experimental exchange rates from this state and allow for a more detailed comparison of experiment with theory.

ACKNOWLEDGMENTS

One of the authors (M.P.A) gratefully acknowledges the National Science Foundation under Grant No. CHE-9504655 for support during the course of this work. One of the authors (P.B.K) thanks the NIEHS Superfund Basic Research Program (Grant No. 3-P42-ES04699). One of the authors (M.P.A) is a David and Lucile Packard Foundation and Alfred P. Sloan Foundation Fellow.

[1] U. Buck, F. Huisken, J. Schleusener, and H. Pauly, Phys. Rev. Lett. **38**, 680 (1977).
[2] U. Buck, F. Huisken, J. Schleusener, and J. Schaefer, J. Chem. Phys. **74**, 535 (1981).
[3] U. Buck, F. Huisken, G. Maneke, and J. Schaefer, J. Chem. Phys. **78**, 4430 (1983).
[4] J. Schaefer and W. Meyer, J. Chem. Phys. **70**, 344 (1979).
[5] W. Meier, G. Ahlers, and H. Zacharias, J. Chem. Phys. **85**, 2599 (1986).
[6] R. L. Farrow and D. W. Chandler, J. Chem. Phys. **89**, 1994 (1988).
[7] J. Arnold, T. Dreier, and D. W. Chandler, Chem. Phys. **133**, 123 (1989).
[8] T. G. Kreutz, J. Gelfand, R. B. Miles, and H. Rabitz, Chem. Phys. **124**, 359 (1988).
[9] N. G. Dautov and A. M. Starik, High Temp. **32**, 210 (1994).
[10] J. M. Ogden, M. M. Steinbugler, and T. G. Kreutz, J. Power Sources **79**, 143 (1999).
[11] C. E. Thomas, B. D. James, F. D. Lomax, Jr., and I. F. Kuhn, Jr., Int. J. Hydrogen Energy **25**, 551 (2000).
[12] N. M. Marinov, H. J. Curran, W. J. Pitz, and C. K. Westbrook, Energy Fuels **12**, 78 (1998).
[13] P. Van Blarigan, Energy Fuels **12**, 72 (1998).
[14] G. A. Pavlov and A. A. Shiryaev, Izv. Akad. Nauk SSSR, Mekh. Zhidk. Gaza 163 (1985).
[15] R. Lacalli and H. Oman, Proceedings of the 23rd Intersociety Energy Conversion Engineering Conference, Denver, Colarado, 31 July–4 August 1998, p. 369.

[16] S. M. Cureton, S. Vyas, P. B. Kelly, and M. P. Augustine, Mol. Phys. **98**, 349 (2000).
[17] C. Schwartz and R. J. Le Roy, J. Mol. Spectrosc. **121**, 420 (1987).
[18] It is important to note that the energy gap model that is often used to understand rotational energy transfer is not used here. Since the vibrational energy spacing is so large in H_2, the energy defect between molecules in different rotational states yields a negligible effect in the overall vibrational exchange rate.
[19] K. E. Shuler, J. Chem. Phys. **32**, 1692 (1960).
[20] J. O. Hirschfelder, C. F. Curtiss, and R. Bryon Bird, *Molecular Theory of Gases and Liquids* (Wiley, New York, 1954).
[21] G. C. Light, J. Chem. Phys. **68**, 2831 (1978).